Structure, Volume *23*

Supplemental Information

Structural Dynamics of Ribosome Subunit Association Studied by Mixing-Spraying Time-Resolved Cryogenic Electron Microscopy

Bo Chen, Sandip Kaledhonkar, Ming Sun, Bingxin Shen, Zonghuan Lu, David Barnard, Toh-Ming Lu, Ruben L. Gonzalez, and Joachim Frank

SUPPLEMENTAL INFORMATION

SUPPLEMENTAL FIGURES and LEGENDS

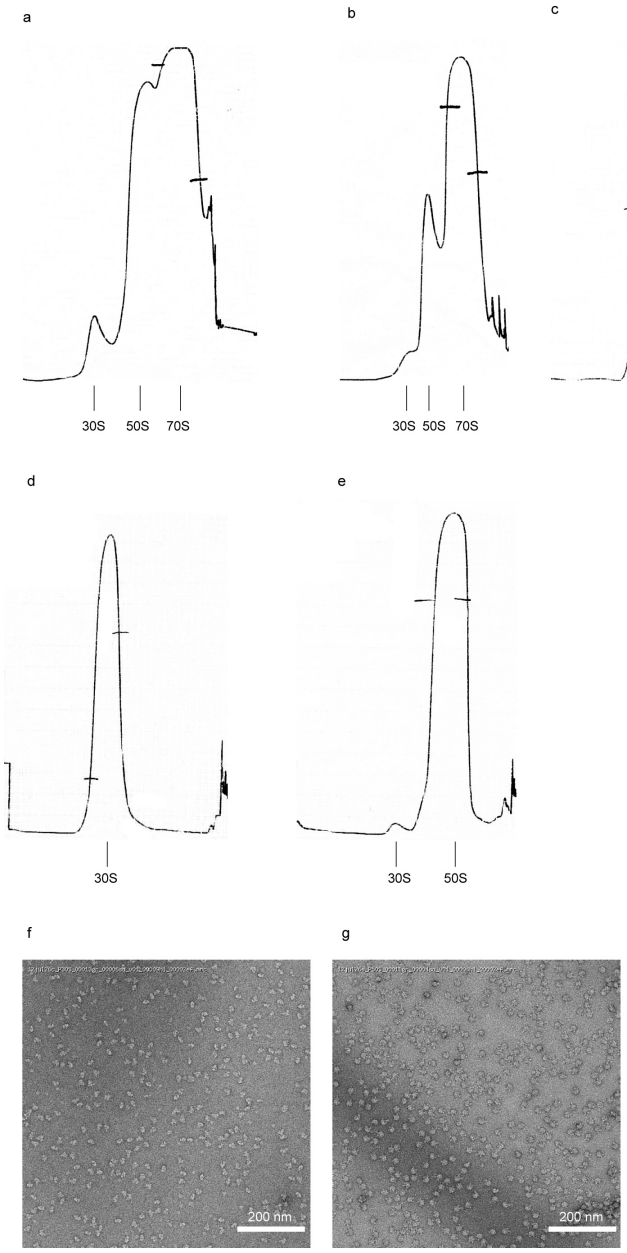

Figure S1. Ribosome subunit purification. Related to **Figure 2**. (a, b) Profiles of the first and second round of sucrose gradient in the presence of 7.5 mM Mg^{2+} to isolate tight-coupled 70S ribosome. (c) Profile of the third round of sucrose gradient in the presence of

1.0 mM Mg^{2+} to split tight-coupled 70S ribosome into 30S and 50S subunits. (d, e) Profiles of the fourth round of sucrose gradient in the presence of 1.0 mM Mg^{2+} to isolate 30S subunit and 50S subunit, respectively. (f, g) EM images of negatively stained samples of 30S subunits and 50S subunits, respectively.

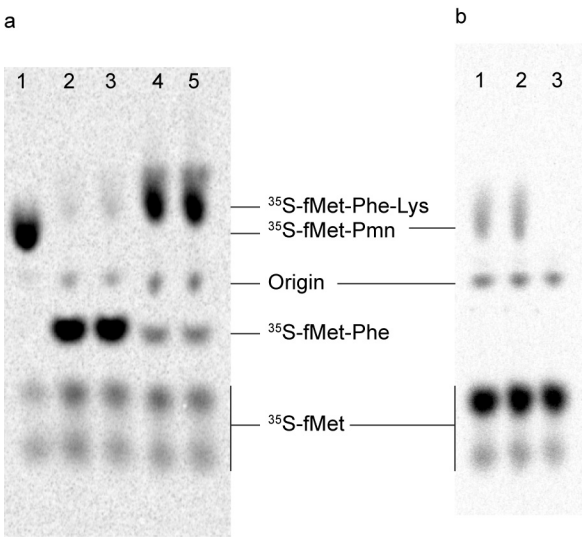

Figure S2. Translation activity assays for the associated ribosome complex. Related to **Figure 2**. (a) Tripeptide formation assay for the associated ribosome formed from the purified 30S and 50S subunits (see Experimental Procedures for details). Lane 1: added puromycin (Pmn) to the 70S initiation complex (IC), and incubated at 37°C for 1 min. Lanes 2 and lane 3: added ternary complexes of $tRNA^{Phe}$ and $tRNA^{Lys}$ in the absence of EF-G, and incubated at 37°C for 1 min and 2 min, respectively. Lanes 4 and lane 5: added ternary complexes in the presence of EF-G, and incubated at 37°C for 1 min and 2 min, respectively. (b) Comparison of activity of ribosomes mixed in time-resolved mixing-spraying device versus mixed by pipetting (see Experimental Procedures for details). Lane 1: used 30S/50S mixture collected from the mixing-spraying device to form the 70S translation initiation complex, then added puromycin and incubated at 37°C for 1 min. Lane 2: used the 30S/50S mixture resulting from gently pipetting to form the 70S translation initiation complex, then added puromycin and incubated at 37°C for 1 min. Lane 3: same as lane 1 except done in the absence of puromycin.

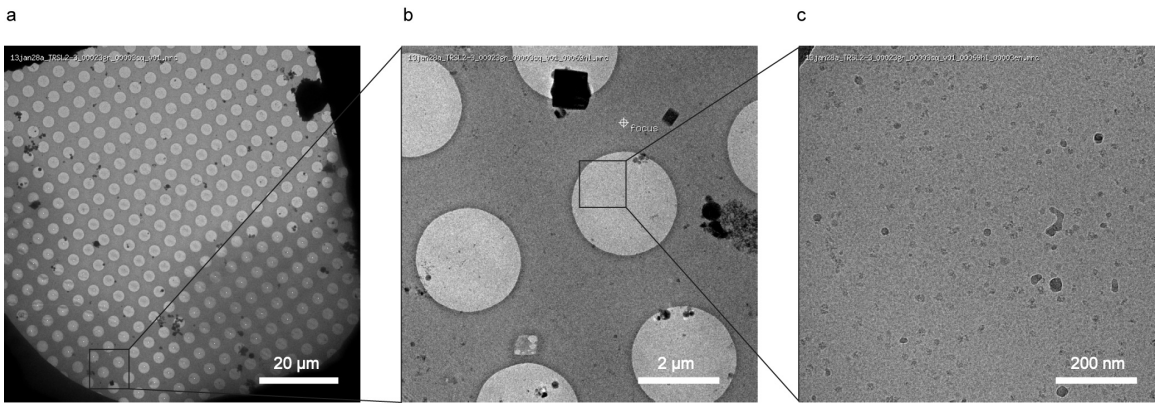

Figure S3. Example of time-resolved cryo-EM images collected using Leginon program. Related to **Figure 1**. (a, b, c) Successive zoom-ins of boxed region in the previous EM image. The ramping effect due to uneven ice thickness, which results in uneven brightness of the image, is negligible in hole (b) and high-magnification (c) images.

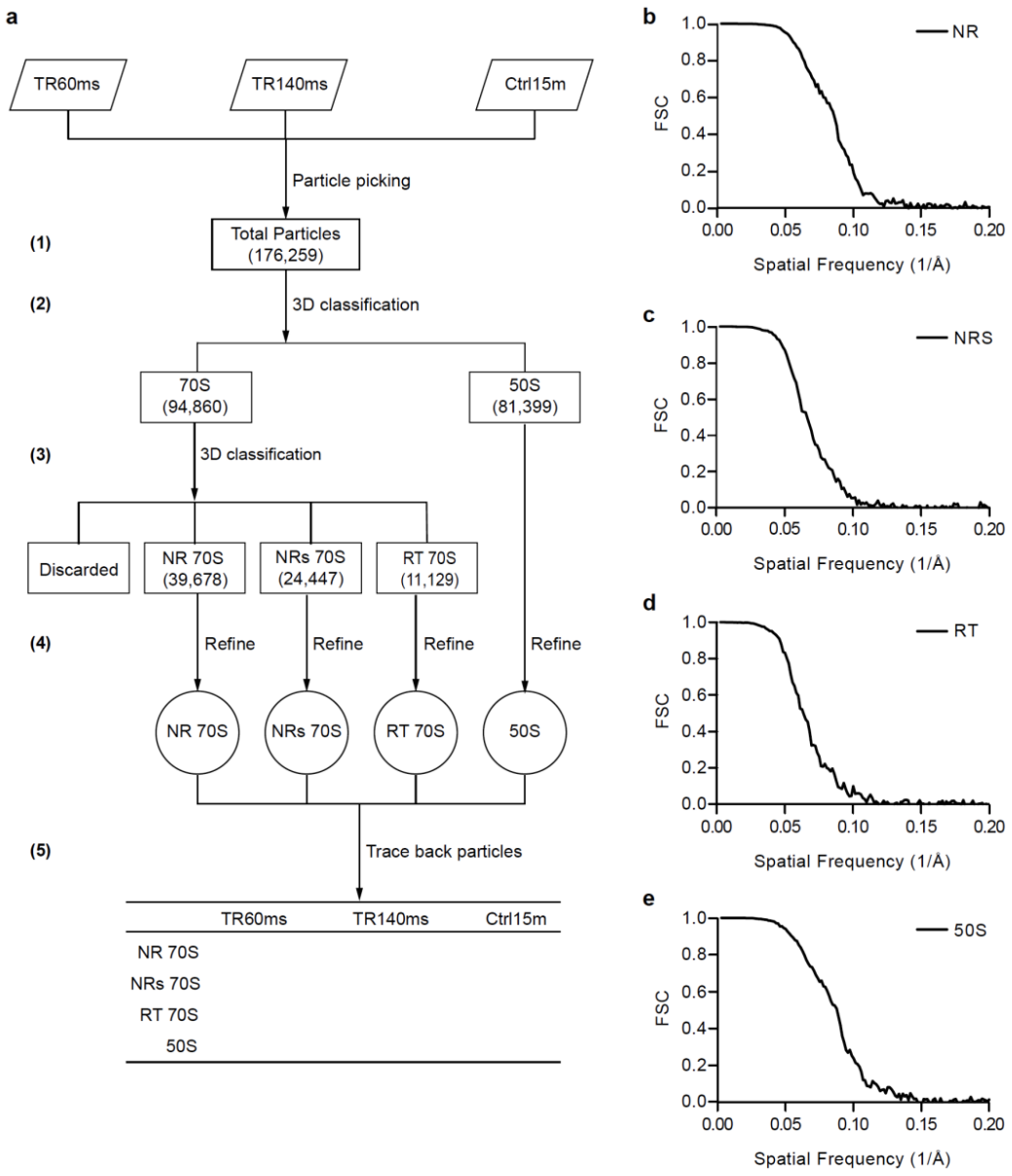

Figure S4. Schematic of single-particle analysis and classification, and the FSC curve for each class. Related to **Figure 3**. (a) Schematic of single-particle analysis and classification. The micrographs of time-resolved and control datasets (top row) were combined for automatic particle-picking. Multiple, step-wise classifications then separated the combined single particles into different classes representing 70S ribosome, the 50S subunit, or bad particles stemmed from noise or contamination on the grid. The

classified particles were then traced back to each dataset to calculate the proportion of 70S ribosomes and 50S subunits (see **Experimental Procedures** – 3D classification). (b-e) The FSC curve for each class of reconstruction: nonrotate (NR) (b), nonrotated with 30S head swivel (NRS) (c), rotated (RT) (d), and 50S subunit (e).

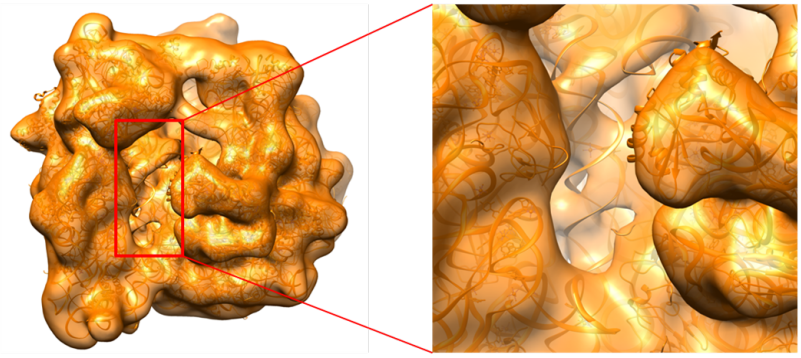

Figure S5. The 3D reconstruction of 70S NR conformation from 5,499 particles in the time-resolved 60 ms dataset. Related to **Figure 4**. Crystallographic structure of 70S ribosome (PDB ID: 2AVY, 2AW4) is rigid-body fitted into the density map for visual aid. The zoom-in image on the right shows a clear density of helix 44 of 30S subunit. Bridges B2a, B3, and B5 are visible in this reconstruction, indicating that these bridges have formed within 60 ms of the ribosome subunit association reaction.

SUPPLEMENTAL TABLES

Table S1. Percentage of 70S ribosome in total 50S-containing particles in each dataset. Related to **Figure 2**.

Percentage (%) [a]	60ms	140 ms	15 minute
50S	66.8 ± 3.4	58.2 ± 2.1	15.3 ± 2.0
70S	33.2 ± 3.4	41.8 ± 2.1	84.8 ± 2.0

[a] The percentage value is shown as average ± standard deviation. Standard deviation is calculated from four runs of RELION 3D classification.

Table S2. Percentage of 70S ribosome in each conformation in total 70S particles in each dataset. Related to **Figure 5**.

Percentage (%) [a]	60 ms	140 ms	15 min
70S NR	61.6 ± 4.1	61.8 ± 5.3	48.0 ± 4.9
70S NRS	27.8 ± 4.5	25.4 ± 5.6	33.1 ± 6.3
70S RT	10.7 ± 0.7	12.8 ± 0.7	18.9 ± 1.6

[a] The percentage value is shown as average ± standard deviation. Standard deviation is calculated from four runs of RELION 3D classification.

SUPPLEMENTAL EXPERIMENTAL PROCEDURES

Kinetic simulation. We simulated the concentration change in the 30S + 50S <=> 70S reaction. The concentration of the 70S ribosome was solved numerically in MATLAB by using $\Delta c(70S) / \Delta t = k_a \times c(30S) \times c(50S) - k_d \times c(70S)$, with an incremental time $\Delta t = 0.5$ ms. We assumed an association rate constant k_a of 13.9 $\mu M^{-1} s^{-1}$, based on previous light-scattering assays (Hennelly et al., 2005), and a dissociation rate constant k_d of 0.002 s^{-1} based on the estimation by Wishnia and coworkers (Wishnia et al., 1975). In the sub-second time range, the dissociation of 70S ribosome is negligible in the kinetic simulation. The simulation starts (t = 0 s) when 1.2 μM 30S and 0.6 μM 50S (both final concentration after mixing) are mixed thoroughly.

Buffers. For ribosome storage, we used Tris-M3.5 buffer (25 mM Tris-HCl, pH 7.6, 60 mM NH_4Cl, 5 mM 2-mercaptoethanol, 3.5 mM $MgCl_2$). For negative staining EM experiments, we used Tris-M10 buffer (25 mM Tris-HCl, pH 7.6, 60 mM NH_4Cl, 5 mM 2-mercaptoethanol, 10 mM $MgCl_2$). For peptide synthesis assay, we used PolyMix-M7 buffer (50 mM Tris acetate, pH 7.0 at 25 °C, 100 mM KCl, 5 mM NH_4OAc, 7 mM $Mg(OAc)_2$, 0.5 mM $Ca(OAc)_2$, 0.1 mM EDTA, 10 mM 2-mercaptoethanol, 5 mM putrescine dihydrochloride, 1 mM spermidine free base). For preparing time-resolved cryo-EM grids, we used HEPES-M12 buffer (20 mM HEPES-KOH, 30 mM NH_4Cl, 5 mM 2-mercaptoethanol, 12 mM $MgCl_2$) to induce spontaneous ribosome subunit association, in the absence of mRNA, initiator tRNA and initiation factors.

Ribosome subunit purification. Ribosome subunits of the tight-coupled 70S ribosomes were purified using sucrose density gradient as describe previously (Fei et al., 2010). Specifically, tight-coupled 70S ribosome from *E. coli* strain MRE600 was isolated

from the rest of the cell components at 7.5 mM Mg^{2+} concentration, and then split to the subunits via dialysis against the buffer containing 1.0 mM Mg^{2+}.

Check for purity of ribosome subunits by negative staining EM. Samples of 30S and 50S subunits each was diluted to 1.2 μM using Tris-M10 buffer, and incubated at 37 ˚C for 15 min, then diluted to 30 nM using Tris-M10 buffer just before application to the EM grid. 5 μL of each specimen was applied on the EM grid for 30 sec, then wicked off by filter paper. 3 μL 2% uranium acetate was then applied to the EM grid for 30 sec, wicked off by filter paper. The staining process was repeated for three times total. The resulting negative staining EM grids were stored at room temperature and examined on the F20 TEM.

Assay of peptide synthesis activity of the associated ribosomes using electrophoretic thin-layer chromatography (eTLC). The polypeptide synthesis assay was performed as previously described (Fei et al., 2010), with minor alterations. Specifically, to test the translation activity of the purified ribosome subunits, we used the f-[^{35}S]Met-Phe-Lys tripeptide assay. The initiation complex mix contained (final concentration of each component in the peptide synthesis reaction, in the order of adding reagents, the same below), in PolyMix-M7 buffer: 0.6 μM IF1, 0.6 μM IF2, 0.6 μM IF3, 1 mM GTP, 0.4 μM 30S (or 50S, or both purified subunits mixed by gentle pipetting, the concentration determined by light absorption at 260 nm), 0.8 μM mRNA (pT7gp32 mRNA coding for Met-Phe-Lys-Glu), and 0.2 μM f-[^{35}S]Met-tRNA^{fMet}. The ternary complex mix contained 8 μM EF-Tu, 1 μM EF-Ts, 1 mM GTP, 0.8 μM Lys-tRNA^{Lys}, 0.8 μM Phe-tRNA^{Phe}. The EF-G mix contained 1 mM GTP, 1.6 μM EF-G. Each peptide synthesis reaction was performed by mixing 2 μL initiation complex with 1.6 μL ternary

complex mix, then with 0.4 μL EF-G mix (or buffer), and incubating at 37 ˚C for 2 min (unless otherwise indicated), then quenching with 0.5 mM KOH to 160 mM final concentration. The eTLC is performed as previously described (Fei et al., 2010; Youngman et al., 2004). The reactants and products on the resulting eTLC were quantified using the phosphor imager. The peptide formation efficiency (E_{pep}) was calculated by using: $E_{pep} = I_{tripeptide} / (I_{tripeptide} + I_{dipeptide})$, where $I_{dipeptide}$, $I_{tripeptide}$ represents the integrated intensity of the spot on the phosphor image corresponding to f-[^{35}S]Met-Phe, f-[^{35}S]Met-Phe-Lys, respectively. When incubated without EF-G mix, E_{pep} = 10% (1 min) and 13% (2 min); when incubated with EF-G mix, E_{pep} = 81% (1 min) and 82% (2 min).

Assay by puromycin reaction. Furthermore, to compare the translation activity of ribosome subunit mixed in the time-resolved device *vs.* mixed by pipetting, we used the f-[^{35}S]Met-puromycin (Pmn) formation assay. The puromycin reaction reports the total amount of ribosome-bound P-site f-[^{35}S]Met-tRNA^{fMet} that is competent for the peptide transfer reaction. The initiation complex mix contained (final concentration): 0.5 mM GTP, 0.45 μM IF1, 0.45 μM IF2, 0.45 μM IF3, 0.3 μM f-[^{35}S]Met-tRNA^{fMet}, 0.9 μM mRNA, and ribosome subunit mixture (0.39 μM 30S and 0.19 μM 50S, concentration determined by light absorption at 260 nm). The puromycin mix contained 1 mM Pmn. The puromycin reaction was performed by mixing 2 μL initiation complex mix with 2 μL Pmn mix (or buffer, if indicated), and incubating at 37 ˚C for 1 min, then quenching with 1 M KOH to 330 mM final concentration. The eTLC was performed as previously described (Fei et al., 2010; Youngman et al., 2004). The f-[^{35}S]Met-Pmn formation efficiency (E) was calculated by using: $E = I_{fMet\text{-}Pmn} / (I_{fMet\text{-}Pmn} + I_{fMet})$, where $I_{fMet\text{-}Pmn}$,

I_{fMet} represents the integrated intensity of the spot on the phosphor image corresponding to f-[^{35}S]Met-Pmn, f-[^{35}S]Met, respectively. When mixed in the time-resolved device, E = 8.0%; when mixed by pipetting, E = 8.5%.

Purity and activity of ribosome subunits. We purified the ribosome subunits from *E coli* MRE600 strain using sucrose density gradient ultracentrifugation (**Figure S1a–S1e**). The first and second round of ultracentrifugation used a Tris-polymix buffer system containing 7.5 mM Mg^{2+} to isolate tight-coupled 70S ribosomes. The third and fourth round of ultracentrifugation used a Tris-polymix buffer system containing 1 mM Mg^{2+} to dissociate the tight-coupled 70S ribosomes into their component 30S and 50S subunits. The ribosome profile of the fourth round of sucrose density gradients showed clear separation of the 30S and 50S subunits (**Figure S1d–S1e**). We also performed negative-staining EM on the purified subunits to further confirm their purity. The micrographs of the 30S and 50S subunit fractions showed particles exclusively in the elongated shape (characteristic for the 30S subunit) and in the crown view (characteristic for the 50S subunit), respectively (**Figure S1f–S1G**), confirming that the ribosomal subunits prepared for the time-resolved cryo-EM experiment are indeed pure.

We then tested the translation activity of associated 70S ribosomes formed from the purified ribosomal subunits using a peptide synthesis assay. The results showed that the associated 70S ribosomes are able to convert 81% of radioactively labeled f[^{35}S]Met-tRNA^{fMet} into a tripeptide in the peptide synthesis reaction performed in the presence of elongation factor G (EF-G), compared to only 10% conversion in the absence of EF-G, thereby confirming the high functional activity of the associated 70S ribosomes (**Figure S2a**). Moreover, we also demonstrated that mixing the subunits in the mixing-spraying

device, followed by spraying the resulting 70S ribosomes, does not affect the translation activity of the associated 70S ribosomes, as it is comparable to the translation activity of ribosomes obtained by mixing the subunits *outside* the device by gently pipetting (**Figure S2b**).

Breakdown of reaction time in time-resolved cryo-EM experiment. (1) The reaction time has a finite distribution, which was estimated by fluid dynamic simulation. For the chip having a mean reaction time of 38 ms (calculated by dividing the total volume of the reaction channel by the total flow rate), the most populated reaction time (peak time) is about 27-31 ms. The cumulative fractions of the solution having a reaction time no more than a cut-off time (in parentheses) are: 20% (29 ms), 40% (31 ms), 60% (38 ms), 80% (57 ms). For the chip having a mean reaction time of 107 ms, the peak time is about 67-73 ms. The cumulative fractions of the solution and the cut-off times (in parentheses) are: 20% (69 ms), 40% (76 ms), 60% (88 ms), and 80% (126 ms). (2) Droplets take less than (10 mm / (6 μl/s / 30 μm / 40 μm) =) 2 ms to fly to the EM grid. (3) After the droplets have hit the EM grid, it takes (35 mm / 1.0 m/s =) 35 ms to plunge the EM grid into liquid ethane at 1.0 m/s plunging velocity (calibrated speed of stepping motor) when performing the experiments using the 107 ms chip. It takes 18 ms at 2.0 m/s when using the 60 ms chip. (4) Once grid is immersed in cryogen, freezing takes ~ 0.1 ms (Cyrklaff et al., 1990). Therefore, the total mean reaction time is 107 ms + 2 ms + 35 ms + 0.1 ms ~ 144 ms for the 107 ms chip (i.e., approximately 140 ms), and 38 ms + 2 ms + 18 ms + 0.1 ms ~ 58 ms for the 38 ms chip (approximately 60 ms).

Preparation of control cryo-EM grids using the blotting method. In control experiments, we used the same batch of purified ribosome subunits as used in time-

resolved cryo-EM experiment, and prepared cryo-EM specimens using the standard blotting method. The 30S and 50S subunits were mixed by gentle pipetting at the same concentration as the time-resolved experiment (1.2 μM 30S and 0.6 μM 50S), incubated at 37˚C for indicated time (15 min or 75 min), then diluted using HEPES-M12 buffer (or Tris-M10 buffer, if indicated) to about 30 nM 50S concentration within 5 min before preparing the cryo-EM specimens using Vitrobot Mark IV (FEI, Hillsboro, Oregon).

Automatic particle-picking. We kept 2,586 good micrographs for the time-resolved cryo-EM 140 ms dataset, characterized as having visible ribosome particles and round Thon rings extended to about 15-12 Å by visual examination. These good micrographs were comparable in quality with cryo-EM images obtained in the control experiments with the blotting method. We also kept 453, 264, and 1019 good micrographs from the Ctrl 15 min, Ctrl 75 min, and Ctrl 15 min Tris datasets, respectively. We then pooled all the good micrographs from all four experiments together, and used an automatic particle-picking program Autopicker (Langlois et al., 2014) to select a total of 906,896 putative particles (i.e., 50S subunits, 70S ribosomes, ice blobs, and any other particles). 70S ribosome and 50S subunit are both selected by the program because they are similar in size and shape (as compared to the 30S subunit). Using the same parameters as the abovementioned pooled dataset, putative particles were also picked from 816 micrographs of the 60 ms dataset. Although some dimers of 50S:50S and trimers of 50S:30S:30S were observed on the micrographs (see Shaikh et al., 2014 (Shaikh et al., 2014)), they were excluded from downstream processing through control of the selection window size in Autopicker (Langlois et al., 2014).

Initial 3D classification by using RELION. In the first classification to ascertain that the time-resolved method can capture a pre-equilibrium state of the subunit association reaction, we pooled the 140 ms dataset with three control datasets (Ctrl 15 min, Ctrl 75 min, and Ctrl Tris 15 min), classified the dataset computationally using the program RELION (Scheres, 2012; Scheres, 2011), and then traced back each particle to its original dataset. The purpose of pooling the datasets into a single dataset is to classify all the data using the same criterion, so that the proportions of subpopulations in the datasets are comparable. The 50S and 70S particles were traced back to quantify the proportion of 70S in 50S-containing particles and the proportion of each 70S conformation in the total 70S particles in each experiment. However, it is important to note that if the proportion of 70S ribosomes in intermediate conformations is small in the time-resolved 140 ms dataset, pooling it with the three control datasets will further decrease the proportion of such intermediates, resulting in higher risk of missing the discovery of such intermediate conformations. To overcome this shortcoming, we removed two control datasets (Ctrl 75 min and Ctrl Tris 15 min) and included the 60 ms time-resolved dataset to perform the second classification described in the main text.

In the first classification of the combined dataset including 140 ms, 15 min, 75 min and Tris 15 min data, we used the RELION program in a stepwise hierarchical classification to discard bad particles identified by the automatic particle-picking program, to separate the 50S subunit from the 70S ribosome, and to sort out the various conformations of the 70S ribosome. The reference volume for the initial alignment of the total dataset of putative particles was chosen to be a 50S subunit density map (the cryo-EM map of empty 70S ribosome (Valle et al., 2003) with 30S subunit computationally

removed), low-pass filtered to 60 Å. To speed up the classification, we used the particle data in twofold decimated form for classification, and used the data in un-decimated form only in the final steps of 3D reconstruction and refinement.

In step (1), the total dataset (906,896 particles) was separated into 12 classes using RELION 3D classification with a 7.5˚ angular sampling interval. The classification results were analyzed using a quantitative analysis method (Shen et al., 2014), and the reconstructions from the different classes were examined by using UCSF Chimera (Pettersen et al., 2004) program. The classes resulting in bad reconstructions (i.e., particles fragmented or unrecognizable; 210,848 particles in total) were discarded. The classes yielding a reconstruction of either 70S ribosome or 50S were kept for step (2) of the classification. In step (2), the remaining particles (696,048 particles) were classified into 12 classes. Classes yielding reconstructions of 70S ribosomes (478,383 particles) were separated from the classes yielding 50S subunits (217,665 particles). In step (3), the classes from the second step yielding 70S reconstructions (478,383 particles) were classified into 10 classes, and the classes resulting in bad reconstructions, likely due to remaining unrecognizable particles, were discarded, keeping 272,717 particles of 70S ribosomes. In step (4), the classes from step (2) yielding 50S reconstructions (217,665 particles) were classified into 8 classes, and the classes yielding reconstructions of 50S subunits were kept (97,338 particles). In step (5), the computationally cleaned 70S particles from step (3) (272,717 particles) were pooled together for 3D auto-refinement, to align the particles to a common reference volume of the 70S ribosome from step (2). Then the aligned particles were classified into 12 classes using a 1.8˚ angular sampling interval. The classes were regrouped based on their resulting reconstructions: non-rotated

70S (NR) (83,877 particles), non-rotated 70S with 30S-head swivel (NRS) (87,169 particles), and rotated 70S (RT) (81,449 particles). In step (6), each class of 70S ribosomes or 50S subunits was refined using 3D auto-refinement with data in un-decimated form. In step (7), the particles were tracked back to each experiment, to quantify the percentage of 70S and the proportion of 70S in each conformation.

The proportions of 70S in 50S-containing particles are: 45% (140 ms), 89% (Ctrl 15 min), 95% (Ctrl 75 min), 86% (Ctrl 15 min Tris). The proportion of 70S ribosomes in the 140 ms data set is much lower than that in the Ctrl 15 min experiment, indicating that the time-resolved 140 ms experiment captured a pre-equilibrium state of the ribosome subunit association reaction. The proportions of 70S in different conformations are omitted to avoid confusion, because they are not directly comparable with those in the second classification combining 60 ms, 140 ms and Ctrl 15 min data.

A comparison of the two control datasets appears to suggest that the proportion of 70S ribosomes increases with longer incubation time, incompatible with our plausible assumption that both Ctrl 15 min and Ctrl 75 min datasets represent the equilibrium state of the subunit association reaction. Although some technical limitations may affect the accuracy of the proportions of 70S particles (see **Strategy for classification**), it is possible that the 70S formation reaction has a slow phase (for some or all the ribosomal subunits) that proceeds even after 15 min incubation at 37˚C, since the previous kinetic studies focused on only the first tens of seconds of the reaction (Antoun et al., 2004; Goerisch et al., 1976; Hennelly et al., 2005; Wishnia et al., 1975). Nonetheless, we consider the Ctrl 15 min experiment the equilibrium state of the subunit association

reaction, which has been characterized previously (Antoun et al., 2004; Hennelly et al., 2005).

Technical limitations that may affect the accuracy of estimating the proportions. We note that the accuracy of estimating the proportions may be affected by two technical limitations. First, in the particle selection step, not all the 70S ribosomes and 50S subunits present in a micrograph will be selected by the particle-picking program, because particles that are too close to each other are excluded. Second, in the classification procedure, some otherwise acceptable particles may be incorrectly classified to a class mainly containing unacceptable particles (e.g., ice splotches or some other form of contamination) with an inferior average image (during 2D classification) or an inferior 3D reconstruction (during 3D classification) and consequently discarded before the final 3D reconstruction. Due to such limitations, the attrition rates of acceptable 70S ribosomes and 50S subunits may be different, affecting the calculation of proportions. Nonetheless, these systematic errors affect the population counts at the three time points equally, and they will not interfere with the observation of time dependence.

Estimation of the dissociation constant and the equilibrium concentration of 70S ribosome. Consider the reaction 30S + 50S <=> 70S. The dissociation constant $K_D = k_d / k_a = [30S]\,[50S] / [70S]$, where k_d and k_a are the dissociation and association rate constants, [x] denotes the equilibrium concentration of x. Assume (1) the measured starting concentrations of the ribosomal subunits are accurate; (2) all subunits are active for the association reaction; (3) K_D is independent on the starting concentrations of ribosome subunits, given the ambient temperature and buffer conditions.

Starting concentrations of the subunits (after mixing, the same below) in the time-resolved experiments without dilution are $c_0(30S)$ = 1.2 μM, $c_0(50S)$ = 0.6 μM. At equilibrium,

$$K_D = [30S]\,[50S] / [70S] \qquad (1)$$

$$[50S] + [70S] = c_0(50S) \qquad (2)$$

$$[30S] + [70S] = c_0(30S) \qquad (3)$$

Starting concentrations of the subunits in the blotting experiments with 20× dilution are $c_{d0}(30S)$ = 0.06 μM, $c_{d0}(50S)$ = 0.03 μM. At equilibrium,

$$K_D = [30S]_d\,[50S]_d / [70S]_d \qquad (4)$$

$$[50S]_d + [70S]_d = c_{d0}(50S) \qquad (5)$$

$$[30S]_d + [70S]_d = c_{d0}(30S) \qquad (6)$$

From the Ctrl 15 min experiment, we observed $[70S]_d / c_{d0}(50S) = 0.85$.

To solve for [70S], we first calculate $K_D = 6.1\times10^{-9}$ M^{-1} using equations (4) – (6).

Second, using equations (1) – (3), we solve for [70S] the quadratic equation:

$$K_D = (c_0(30S) - [70S])\,(c_0(50S) - [70S]) / [70S].$$

Because $0 \le [70S] \le c_0(50S)$, there is a unique analytic solution:

$$[70S] = c_0(50S) \times [(m+1+r) - \mathrm{sqrt}\,((m+1+r)^2 - 4\times m)] / 2,$$

where $m = c_0(30S) / c_0(50S)$, $r = (m - p)\,(1 - p) / p \times c_{d0}(50S) / c_0(50S)$, $p = [70S]_d / c_{d0}(50S)$, and sqrt denotes the square root operation.

The numerical solution is $[70S] = 0.990 \times c_0(50S)$.

Segmentation of the maps. We first performed amplitude-correction by using the EM-bfactor program (Fernández et al., 2008; Rosenthal and Henderson, 2003) and low-pass filtered the reconstruction of each class from step (4) of computational classification,

yielding the "final" maps. We then segmented each final map in UCSF Chimera (Pettersen et al., 2004) with the aid of known crystallographic structures of 70S ribosomes (PDB ID: 2AVY, 2AW4, 2AW7, 2AWB) (Schuwirth et al., 2005).

Measurement of 30S subunit rotation. The difference in rotation of the 30S ribosomal subunit between two different 70S ribosomes was measured in UCSF Chimera using inertial axes (Pettersen et al., 2004). We first fitted the two 70S maps on a common 50S subunit reference map, and then fitted a common crystallographic structure of 30S subunit into each 70S map. We then calculated inertial axes of all the phosphate atoms in the two fitted 30S structures, respectively, and measured the rotation angle between the two inertial axes.

Additional comparison between our results and the previous time-resolved cryo-EM study by Shaikh et al. (2014). The first difference between the results presented here and those reported previously by Shaikh and coworkers is that those authors observed a number of 50S dimers and 50S·30S·30S heterotrimer complexes in their 9.4 ms reaction time data. Although inspection of our micrographs showed some instances of such complexes, we chose to concentrate on 50S and 70S particles only, by setting the parameter in the particle-picking program Autopicker (Langlois et al., 2014) to discard particles bigger than the 70S ribosome.

Second, the proportions of 70S ribosome observed by Shaikh and coworkers are higher than those expected from the kinetic simulation with a k_a of 14 $\mu M^{-1} s^{-1}$ (Shaikh et al., 2014). Specifically, the observed proportions of 70S ribosomes in their experiments were 24.7% at 9.4 ms and 48.7% at 43 ms, compared with 11.6% and 37.5% expected from the kinetic simulation, respectively. In contrast, our observed proportions of 70S

ribosome at 60ms and 140 ms are lower than those expected from the kinetic simulation with a k_a of 13.9 μM^{-1} s^{-1} (see **Results – Time course of the subunit association reaction**). Some differences in the experimental conditions may contribute to this discrepancy, such as different activities of the ribosome sample, different ratios of 30S:50S subunits (they used 1:1, we used 2:1 ratio), and the absence or presence of the environmental chamber.

SUPPLEMENTAL REFERENCES

Antoun, A., Pavlov, M.Y., Tenson, T., and Ehrenberg, M. (2004). Ribosome formation from subunits studied by stopped-flow and rayleigh light scattering. Biol. Proced. Online *6*, 35-54.

Cyrklaff, M., Adrian, M., and Dubochet, J. (1990). Evaporation during preparation of unsupported thin vitrified aqueous layers for cryo-electron microscopy. J. Electron. Microsc. Tech. *16*, 351-355.

Fei, J., Wang, J., Sternberg, S.H., MacDougall, D.D., Elvekrog, M.M., Pulukkunat, D.K., Englander, M.T., and Gonzalez Jr, R.L. (2010). Chapter 12 - A highly purified, fluorescently labeled *in vitro* translation system for single-molecule studies of protein synthesis. In Methods Enzymol., G.W. Nils, ed. (Academic Press), pp. 221-259.

Fernández, J.J., Luque, D., Castón, J.R., and Carrascosa, J.L. (2008). Sharpening high resolution information in single particle electron cryomicroscopy. J. Struct. Biol. *164*, 170-175.

Goerisch, H., Goss, D.J., and Parkhurst, L.J. (1976). Kinetics of ribosome dissociation and subunit association studied in a light-scattering stopped-flow apparatus. Biochemistry *15*, 5743-5753.

Hennelly, S.P., Antoun, A., Ehrenberg, M., Gualerzi, C.O., Knight, W., Lodmell, J.S., and Hill, W.E. (2005). A time-resolved investigation of ribosomal subunit association. J. Mol. Biol. *346*, 1243-1258.

Langlois, R., Pallesen, J., Ash, J.T., Nam Ho, D., Rubinstein, J.L., and Frank, J. (2014). Automated particle picking for low-contrast macromolecules in cryo-electron microscopy. J. Struct. Biol. *186*, 1-7.

Pettersen, E.F., Goddard, T.D., Huang, C.C., Couch, G.S., Greenblatt, D.M., Meng, E.C., and Ferrin, T.E. (2004). UCSF Chimera—A visualization system for exploratory research and analysis. J. Comput. Chem. *25*, 1605-1612.

Rosenthal, P.B., and Henderson, R. (2003). Optimal determination of particle orientation, absolute hand, and contrast loss in single-particle electron cryomicroscopy. J. Mol. Biol. *333*, 721-745.

Scheres, S.H. (2012). RELION: implementation of a Bayesian approach to cryo-EM structure determination. J. Struct. Biol. *180*, 519-530.

Scheres, S.H.W. (2011). A Bayesian view on cryo-EM structure determination. J. Mol. Biol. *415*, 406-418.

Schuwirth, B.S., Borovinskaya, M.A., Hau, C.W., Zhang, W., Vila-Sanjurjo, A., Holton, J.M., and Cate, J.H.D. (2005). Structures of the bacterial ribosome at 3.5 Å resolution. Science *310*, 827-834.

Shaikh, T.R., Yassin, A.S., Lu, Z., Barnard, D., Meng, X., Lu, T.-M., Wagenknecht, T., and Agrawal, R.K. (2014). Initial bridges between two ribosomal subunits are formed within 9.4 milliseconds, as studied by time-resolved cryo-EM. Proc. Natl. Acad. Sci. *111*, 9822-9827.

Shen, B., Chen, B., Liao, H., and Frank, J. (2014). Quantitative analysis in iterative classification schemes for cryo-EM applications. In Computational Methods for Three-Dimensional Microscopy Reconstruction, G.T. Herman, and J. Frank, eds. (Birkhauser Basel).

Valle, M., Zavialov, A., Li, W., Stagg, S.M., Sengupta, J., Nielsen, R.C., Nissen, P., Harvey, S.C., Ehrenberg, M., and Frank, J. (2003). Incorporation of aminoacyl-tRNA into the ribosome as seen by cryo-electron microscopy. Nat. Struct. Mol. Biol. *10*, 899-906.

Wishnia, A., Boussert, A., Graffe, M., Dessen, P., and Grunberg-Manago, M. (1975). Kinetics of the reversible association of ribosomal subunits: Stopped-flow studies of the rate law and of the effect of Mg2+. J. Mol. Biol. *93*, 499-515.

Youngman, E.M., Brunelle, J.L., Kochaniak, A.B., and Green, R. (2004). The active site of the ribosome is composed of two layers of conserved nucleotides with distinct roles in peptide bond formation and peptide release. Cell *117*, 589-599.